Nondestructive and High-Recovery-Yield Purification of Single-Walled Carbon Nanotubes by Chemical Functionalization

Yongfu Lian,[†] Yutaka Maeda,[†] Takatsugu Wakahara,[†] Takeshi Akasaka,*[,†] Said Kazaoui,[‡] Nobutsugu Minami,[‡] Tetsuo Shimizu,[‡] Nami Choi,[‡] and Hiroshi Tokumoto[‡,§]

Center for Tsukuba Advanced Research Alliance (TARA Center), University of Tsukuba, Tsukuba, Ibaraki 305-8577, Japan, National Institute of Advanced Industrial Science and Technology, Tsukuba, Ibaraki 305-8562, Japan, and Research Institute for Electronic Science, Hokkaido University, Sapporo 001-0021, Japan

Received: February 12, 2004; In Final Form: April 22, 2004

Raw single-walled carbon nanotubes produced by arc discharge were first treated with $K_2S_2O_8$ in dilute H_2SO_4 solution to generate oxygenated functional groups such as carboxyl, hydroxyl, and carbonyl on varying carbon components. Further functionalization with octadecylamine was carried out via a condensation reaction between an amine group and a carboxyl group with the assistance of dicyclohexylcarbodiimide. The attachment of long alkyl chains leads the sample to be soluble in tetrahydrofuran and other organic solvents. The thus obtained stable dispersion was subjected to dispersion−centrifugation recycles, and then the metal catalysts and varying carbon impurities were separated with carbon nanotubes. The advantage of this procedure lies in high-yield and nondestructive recovery of the target material. Optical absorption spectroscopic and thermogravimetric analyses show that about 60% of the nanotubes in the starting material is extracted with a purity more than 90 wt %.

1. Introduction

Because of their unique one-dimension structure, high surface area, electrical conductivity, and extremely high strength,[1] single-walled carbon nanotubes (SWNTs) are proposed to have many promising applications in nanoelectronics, nanoprobes, nanostructural composites, field-emission displays, chemical sensors, etc.[1,2] To realize these potentials and to study their intrinsic properties, high quality SWNTs are required. Unfortunately, the current methods for large-scale production of SWNTs generate significant amounts of carbonaceous impurities, such as amorphous carbon, fullerene, turbostratic graphite (TSG), and polyhedral carbon nanoparticles (PCNs), along with transition metals that were introduced as catalysts in the growth of nanotubes.[3−5] Despite extensive efforts,[6−19] it is still a challenge to obtain a large amount of SWNTs pure enough for their technological development and scientific study.

Normally, carbonaceous impurities are removed by refluxing raw samples in boiling nitric acid or burning them in air under a relatively high temperature.[6,7] Amorphous carbon can be etched away to some extent during this process, but other forms of carbonaceous impurities, especially TSG and PCNs, could not be removed in this stage because of their stability higher than that of SWNTs.[8] Furthermore, large numbers of SWNTs are also etched away along with amorphous carbon, which leads to a very low yield of recovery and a high degree of degradation of the target material.[8,9] As for metal catalysts, they are usually removed by inorganic acids such as concentrated HCl with the help of filtering and sonication.[10] However, the accessibility of acids to the metal catalytic particles is hampered when the latter are encapsulated in PCNs. Though exposure to moist air or wet Ar/O_2 mixture,[11] ultrasonically doping SWNTs suspension with inorganic nanoparticles,[12] ozone oxidization,[13] and microwave treatment[14,15] can breach the surrounding carbon shell to some degree, the remaining cracked-open carbon shells are not easy to remove since they are strongly bonded to the nanotube ropes. Moreover, under these severe conditions, SWNTs themselves are also attacked and further damage on the remaining walls inevitably takes place.

In recent years, solution chemistry of nanotubes has attracted much attention, and SWNTs have been brought to varying solvents by surfactant-assisted dispersion,[16] noncovalent modification,[17,20,21] and covalent functionalization.[22,23] Such dissolution not only provides an effective approach to bundle exfoliation and chemical processability of SWNTs, but also allows the removal of varying impurities from nanotubes by microfiltration,[16] capillary electrophoresis separation,[17] and chromatographic isolation.[18] Covalent functionalization could be classified into the amidation or esterification of the carboxylic acid groups of oxidized SWNT material and adding reactive groups onto the sidewalls.[22] Georgakilas et al. reported purification of HiPCO carbon nanotubes with the latter approach.[19] Sidewall functionalization has its disadvantage in that significant modification would drastically affect the solution-phase absorption spectroscopy, leading to a complete loss of optical features. Thus, thermal treatment has to be used to recover the missing electronic properties, which in turn results in the re-aggregation, poor dispersibility, and incompatibility of the target material.

Described in the present work is a nondestructive and scalable procedure for dissolution and purification of SWNTs. A raw SWNT sample was successively functionalized with $K_2S_2O_8$ in dilute aqueous H_2SO_4 solution and with octadecylamine (ODA) through a solvent-free functionalization process, in which long alkyl chains were attached on varying carbons via a condensa-

* Corresponding author. Tel & Fax: (81)-298-53-6409. E-mail: akasaka@tara.tsukuba.ac.jp.
[†] University of Tsukuba.
[‡] National Institute of Advanced Industrial Science and Technology.
[§] Hokkaido University.

10.1021/jp049368z CCC: $27.50
Published on Web 05/28/2004

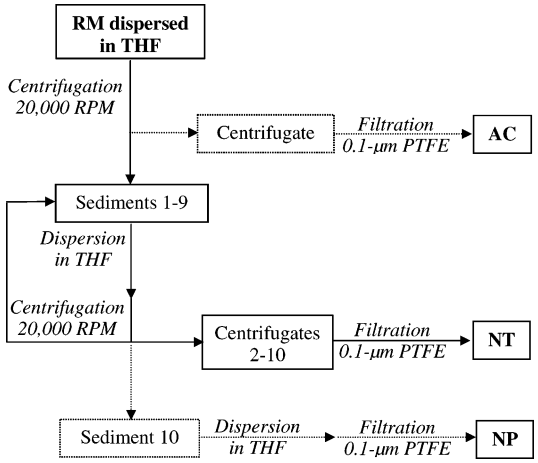

Figure 1. Schematic flowchart of the dispersion−centrifugation cycle.

tion reaction between an amine group and a carboxyl group with the assistance of dicyclohexylcarbodiimide (DCC). Because of their difference in surface area and reactivity, the carbons contained in the starting material should be modified to a varying extent, bringing differences in their solubility. This makes it possible to separate varying carbon impurities and metal catalysts with soluble SWNTs by a centrifuge−dispersion recycle.

2. Experimental Section

A two-step wet chemistry procedure was applied in this work. A 200-mg sample of raw SWNT produced by arc discharge method[3] was first dispersed in 150 mL of aqueous $K_2S_2O_8$ (0.2 M) ultrasonically. After adding 25 mL of 97% H_2SO_4, the mixture was magnetically stirred for 24 h at 60 °C. With the reaction mixture cooled, a SWNT deposit appeared. The upper yellow solution was decanted, and the lower black suspension was further dispersed in 200 mL of distilled water. The decanting−dispersion process was repeated till a stable suspension formed (pH ∼ 6−7). After filtration with a 1-μm poly(tetrafluoroethylene) (PTFE) microfilm and drying for 8 h at 100 °C, a sample that was quite easily dispersible in water, *N*,*N*-dimethylformamide (DMF), and other polar solvents was obtained.

As a second step, the $K_2S_2O_8$-treated sample was further functionalized with a solvent-free process. Into a 100 cm^3 round-bottom flask, 150 mg of $K_2S_2O_8$-treated SWNTs and 7.5 g of ODA were charged. The mixture was heated to 140 °C and stirred with a magnetic stirrer under an Ar atmosphere for a week. After 3 g of DCC was added, the reaction mixture was further heated at the boiling point of DCC for 3 days.

When cooled to room temperature, the reaction mixture (named RM) was dispersed in 500 mL of tetrahydrofuran (THF), and then initially centrifuged at 20 000 rpm for 6 h. The centrifugate was carefully decanted and monitored by a UV−vis−NIR spectrophotometer. The sludge thus obtained was dispersed in a proper amount of THF ultrasonically, and then subjected to further centrifugation. The dispersion−centrifugation process, shown in Figure 1, was repeated till no obvious absorptions from SWNTs were observed in the decanted centrifugate. After 10 dispersion−centrifugation cycles, about two-thirds of the starting material is left as residue, which could not easily be dispersed in THF anymore. The centrifugates obtained were filtered with 0.1-μm PTFE membranes, and the solid samples were dried for 8 h at 100 °C in a vacuum and weighed. We refer to the samples thus obtained as AC, NT, and NP, respectively, which were characterized with the following techniques.

Scanning electron microscope (SEM) observation was carried out with a JEOL JSM-6700FT field emission electron microscope (accelerating voltage: 5.0 kV; beam current: 10 μA). The specimen was fixed to the sample holder via a piece of adhesive carbon tape (DTM 9101, JEOL Datum).

Transmission electron microscope (TEM) analyses were conducted on a Hitachi HD 2000 scanning transmission electron microscope (STEM) equipped with a heating stage (accelerating voltage: 200 kV; beam current: 30 μA). A TEM specimen was prepared by placing several drops of dark THF dispersion of NT or NP onto a tungsten filament, which was heated from room temperature to 300 °C in the sample chamber under a vacuum of ca. 10^{-5} Pa.

Raman spectra were measured with a Jasco NRS-2100 spectrophotometer using laser excitation at 514.5 nm. Specimens were prepared by drying AC, NT, and NP for 1 day in a vacuum at 150 °C.

Atomic force microscopy (AFM) observation was carried out on a Digital Instruments Nanoscope III in the tapping-mode of operation. Well-dispersed soluble SWNTs in DMF or THF were dropped and dried on a freshly cleaved mica surface.

The solution-phase optical absorption data were recorded with a Shimadzu UV-3150 spectrophotometer using a quartz cell with a path length of 10 mm.

Thermogravimetric analysis (TGA) data were recorded with a SII Seiko Instruments EXSTAR 6000 thermogravimetric analyzer. Samples AC, NT, and NP were first heated in argon at a programmed rate of 10 °C/min and a flow rate of 300 mL/min. The residues survived were successively subjected to heating in air at a ramp rate of 5 °C/min and a flow rate of 100 mL/min.

3. Results and Discussion

The purpose of $K_2S_2O_8$ treatment is to oxidize the carbon materials contained in the raw SWNTs sample to a varying extent and to partly remove metal catalysts and amorphous carbon from nanotubes. Though $K_2S_2O_8$ is a strong oxidation reagent in acid medium, it is still a mild chemical to carbon materials because of its usually low chemical reaction rate. Owing to its larger surface area and higher reactivity amorphous carbon is expected to be oxidized to a much higher degree under our reaction conditions than SWNTs and other carbon impurities. The $K_2S_2O_8$-treated sample is quite easily dispersed in water, DMF and other polar solvents, indicating that some hydrophilic groups such as carboxyl and hydroxyl are introduced and tube ropes are unbundled to some extent.

As shown in Figure 2, a representative AFM image of the $K_2S_2O_8$-treated sample, some amorphous carbon is observed on the surface of tube bundles, whereas the length of the latter remains nearly the same as in the pristine material. This means that after the $K_2S_2O_8$ treatment the highly oxidized amorphous carbon is deposited on the surface of SWNTs without obvious damage to the structure of SWNTs. Further support comes from thermogravimetric analysis. Shown in Figure 3 are the TGA and differentiated TGA (DTG) curves of the raw SWNTs and $K_2S_2O_8$-treated SWNTs samples measured in air atmosphere. The weight loss from 100 to 400 °C in Figure 3b corresponds to the removal of hydrophilic groups. Three stepwise weight losses are observed in Figure 3a, whereas only one is detected in Figure 3b. This means that varying carbon components are simultaneously burned after $K_2S_2O_8$ treatment, which is a result of the evenly dispersed amorphous carbon on the surfaces of

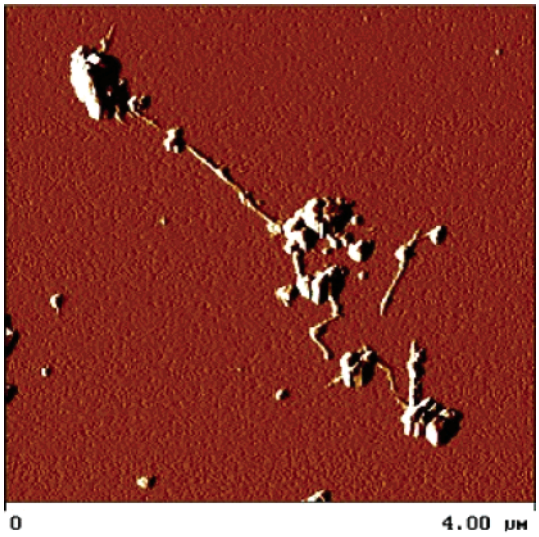

Figure 2. A representative AFM image of the $K_2S_2O_8$-treated SWNT sample dispersed in DMF on a freshly cleaved mica surface observed in the tapping-mode of operation.

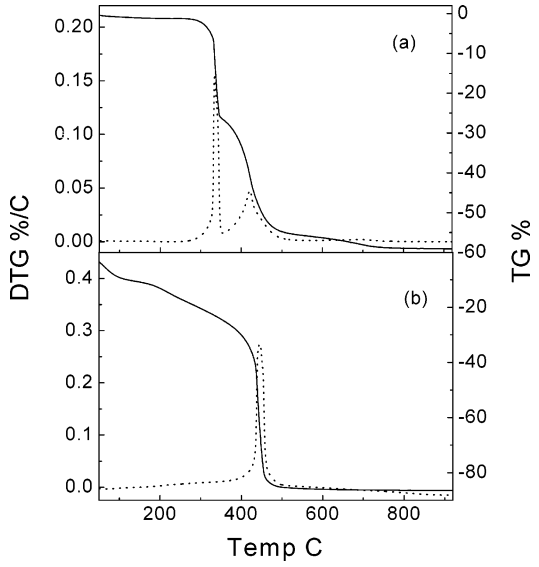

Figure 3. The TGA-DTG curves of (a) the raw and (b) the $K_2S_2O_8$-treated SWNT samples (ramp rate: 5 °C; air flow rate: 100 cm^3/min). The dotted lines represent DTG curves.

SWNTs and other carbon impurities. In addition, the burning of the $K_2S_2O_8$-treated SWNT sample shifts to a higher temperature, which is due to the partial removal of metal catalysts[11] as verified by the smaller amount of residue at 900 °C than that of the raw SWNTs sample. Thus, we suppose that $K_2S_2O_8$ oxidation plays roles in modifying, unbundling and coating SWNTs, which are important for their further functionalization and purification

The morphologies of samples AC, NT, and NP are observed and the degree of purification of SWNTs is qualitatively estimated with a scanning electron microscope. Figure 4 shows the SEM images of samples AC, NT, and NP. From Figure 4a, only irregular agglomerates of amorphous carbon are seen. In contrast, high-density SWNTs are observed in Figure 4b without catalytic metal particles, TSG, or PCNs. It should be noted that the SWNTs are uniformly coated with a sticky material, which should be originated from the attached functional groups alone with a little amorphous carbon residue. Due to the sticky coatings, we could not analyze the length distribution of the SWNT bundles. Nonetheless, bundles with diameters as small

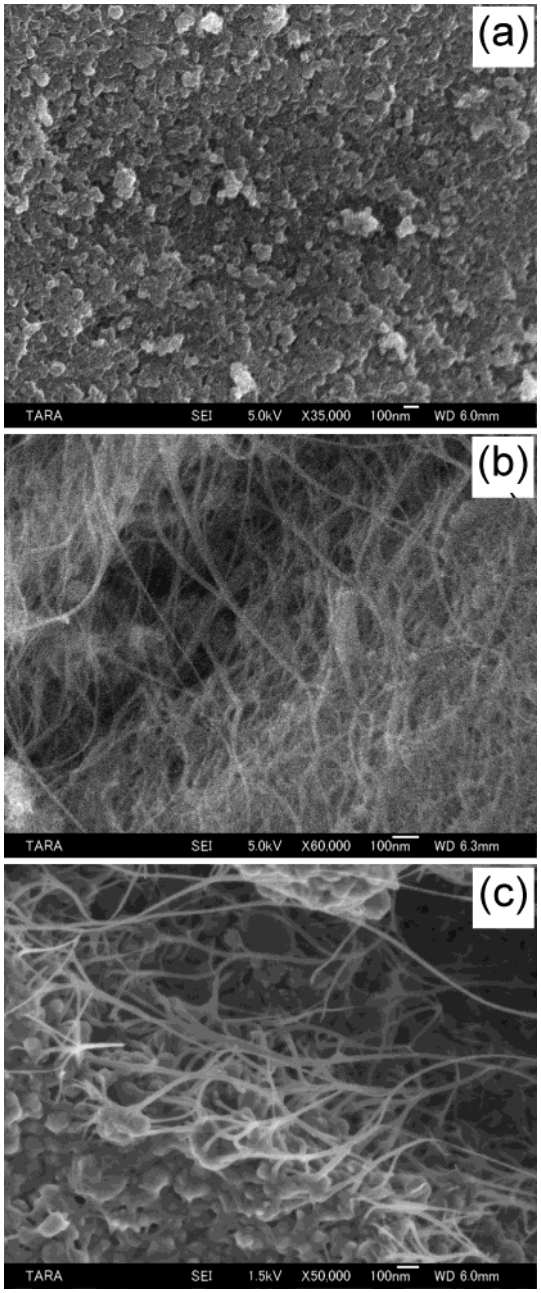

Figure 4. SEM images of samples (a) AC, (b) NT, and (c) NP.

as less than 5 nm are observable in the tear of this sample. Considering the promoting effects of the sticky coatings on the formation of intra- and interbundle bonding, we believe that the functionalized SWNTs could be dispersed in THF individually or as thin bundles. Figure 4c, the SEM image of sample NP, shows a large number of agglomerates of larger particles with a small amount of SWNTs. These particles are thought to be due to metal catalysts, TSG, and PCNs. Of interest to note is that SWNTs in the sample anchor to larger particles through one or both of their ends. They also show cleaner surfaces and larger bundles than those found in Figure 4b, indicating their low degree of functionalization. Therefore, the SEM images clearly reveal that high purity SWNTs are effectively separated with metal catalysts and varying carbon impurities via chemical functionalization and centrifugation.

Raman spectroscopy is a powerful tool to characterize SWNTs. The characteristic peaks, the radial breathing mode (RBM), disordered carbon mode (D band), the tangential Raman mode (split G band), and the combination mode, usually appear

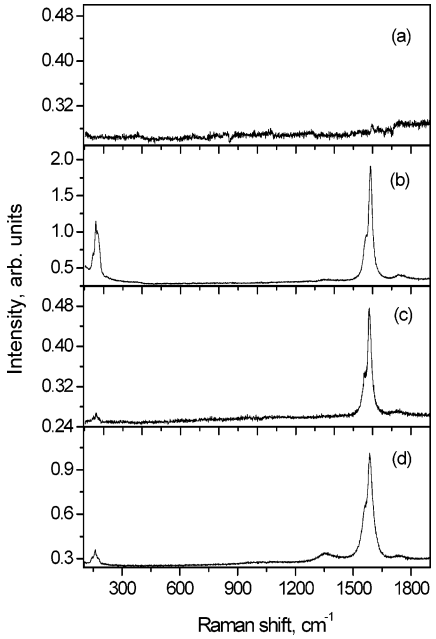

Figure 5. Raman spectra of (a) AC, (b) NT, (c) NP, and (d) as-prepared SWNTs (Jasco NRS-2100 laser Raman spectrophotometer with exciting laser of 514.5 nm).

in the wavenumber ranges in approximately 100−250, 1320−1370, 1530−1610, and 1680−1830 cm^{-1}, respectively.[24,25] Shown in Figure 5 are the Raman spectra of samples AC, NT, and NP. In contrast to Figures 5b and 5c, none of the characteristic Raman peaks are observed in Figure 5a. Thus, it is reasonable for us to ascribe sample AC to highly functionalized amorphous carbon. It is suggested that the area ratios of the Raman peaks (G/D) are proportional to the in-plane crystallite size and inversely proportional to the amount of "unorganized" carbon in graphitic materials.[26,27] As shown in Figures 5b and 5c, the disorder Raman (D) peaks are extremely weak for samples NT and NP with respect to their corresponding prominent split G bands, implying that these samples are well crystallized. Additionally, the weaker D band of sample NP than that of sample NT indicates its lower metamorphic grade. Moreover, the Raman intensity of sample NT is observed about 10 times higher in the RBM, and 4 times higher in the split G band than those of sample NP. Thus, we argue that sample NT is mainly composed of SWNTs and sample NP is enriched in TSG and PCNs along with a few SWNTs.

In comparison with the Raman data of the as-prepared SWNTs shown in Figure 5d, we observed a large increase in the integrated ratio of the Raman peaks (G/D),[27] a reduction in G peak width,[28] and a prominent combination peak[29] near 1744 cm^{-1} in Figure 5b, indicating a dramatic improvement in the SWNT purity of sample NT with respect to the starting material. Moreover, it is well-known that the RBM modes could be used to estimate the diameters and to identify the type (metallic or semiconducting) of SWNTs when resonantly enhanced.[24] As shown in Figures 5b, 5c, and 5d, no observable variance is detected in the distribution of the RBM modes among the starting material, sample NT, and sample NP. Therefore, we conclude that our chemical process causes no or little damage to the structure of SWNTs. Further support comes from the AFM image shown in Figure 6, which does not stand for the whole sample, but has been picked up to show the length of soluble nanotubes. Here, we observed a well-separated thin bundle with length as long as 2.8 μm, which is one order longer than those mixing acids cut ones.[30]

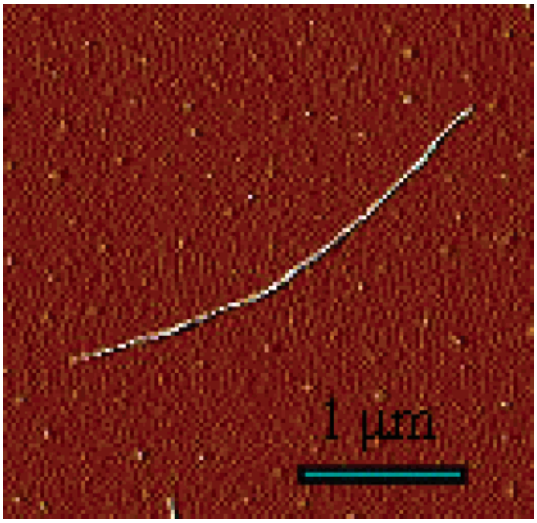

Figure 6. An AFM image of sample NT dispersed in THF on a freshly cleaved mica surface observed in the tapping-mode of operation.

Samples NT and NP were examined by STEM, and typical micrographs are shown in Figure 7. The dark sections in the lower right of Figure 7a and in the lower left of Figures 7b and 7c are due to tungsten filament. A thin and loosely bonded bundle of SWNTs is observed in Figure 7a, and some individual tubes are clearly shown in Figure 7b. This provides direct support to the assumption that the functionalized SWNTs are dispersed in THF individually or as thin bundles. The tube diameter is ~1.4 nm, which is consistent with that determined by optical absorption spectrum.[31] The walls of SWNTs are clean and uniform without nodular deposits. No severe surface roughness as that caused by heavy degree of sidewall functionalization.[32] is detected, though the tubes are evidently coated with some stick materials. Thus, the STEM images directly demonstrate that the chemical purification process causes no or little damage to the structure of SWNTs. From the STEM images of sample NP, catalytic metal particles (see Figure 7c) and polyhedral carbon nanoparticles (see Figure 7d) are frequently observed, which are effectively separated with SWNTs.

In the optical spectra of electric-arc-produced SWNTs, three characteristic absorption bands are usually observed at approximately 1800, 1000, and 700 nm, respectively, superimposed on a broad background.[33] The first two bands are attributed to electronic transitions between the first and second pairs of the van Hove singularities (VHSs) in semiconducting SWNTs, and the last one to the first pair of singularity in metallic SWNTs. Figure 8 shows the absorption spectra of samples AC, NT, and NP in the visible and near-infrared ranges. The above-mentioned optical absorption features are clearly observed in Figures 8b and 8c. However, none of them is detectable in Figure 8a, suggesting that no SWNTs exist in sample AC, which is composed of highly functionalized amorphous carbon. In comparison with those of sample NT, the optical absorption features of sample NP are very weak. In line with the above SEM, STEM, and Raman results, we ascribe sample NP as low-grade modified aggregates of nonnanotube carbon structures such as TSG and PCNs and residual catalyst along with a few large tube bundles.

Chen et al. reported dissolution of purified full-length SWNTs by nitric acid treatment and ODA functionalization.[34] We note here that both the first and the second optical absorption bands originating from semiconducting SWNTs shift to the higher-energy side with respect to ref 34. According to Reich et al.,

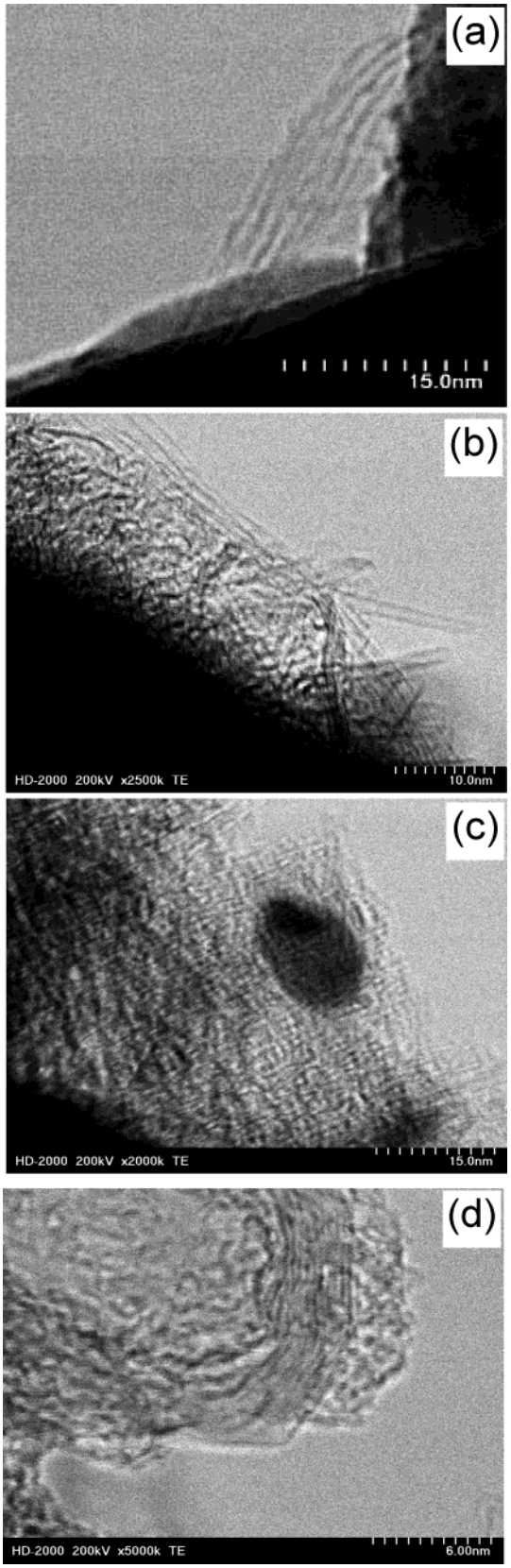

Figure 7. STEM images of samples (a) NT, showing a thin and loosely bonded bundle of SWNTs, (b) NP, showing individual SWNTs, (c) NP, showing a catalytic metal particle, and (d) NP, showing a polyhedral carbon nanoparticle.

bundling of the tubes to ropes will lead to a decrease of the energy gap in semiconducting nanotubes.[35] Moreover, fine structure is also resolved in the visible range of Figure 8b. The features at 644, 675, 699, 735, and 784 nm are ascribed to the

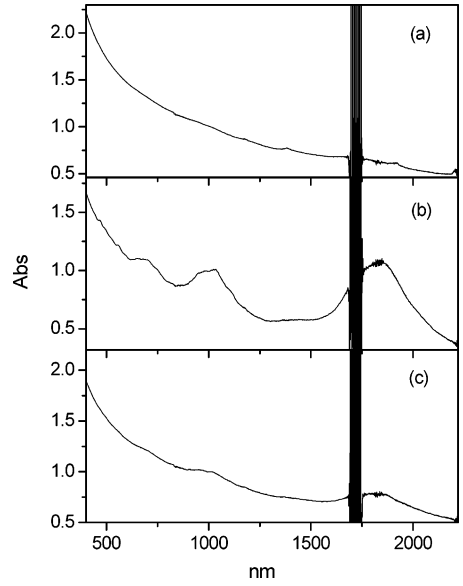

Figure 8. Absorption spectra of (a) AC, (b) NT, and (c) NP, dispersed in THF. To account for the difference in tube concentration, the plots were normalized at 1010 nm.

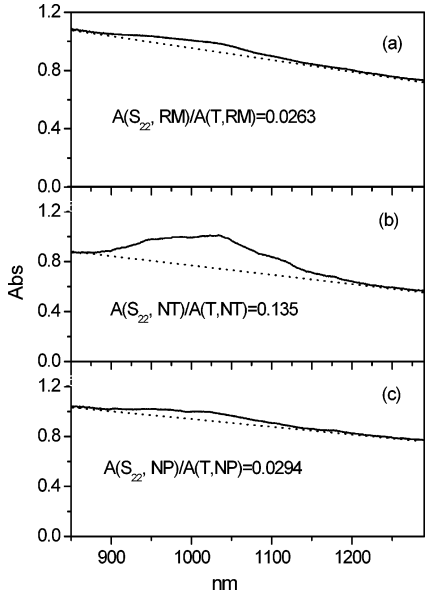

Figure 9. Absorption spectra of (a) RM, (b) NT, and (c) NP dispersed in THF in the range of the S_{22} interband transition. A(T, X) and $A(S_{22}$, X) stand for the total aerial absorption and the aerial absorption of the curve X before and after baseline (dotted lines) subtraction, respectively. To account for the difference in tube concentration, the plots were normalized at 1010 nm.

electronic transitions between the first pair of VHSs in metallic SWNTs, and those at 466, 553, and 584 nm to the third pairs of VHSs in semiconducting SWNTs. The resolution improvement in optical adsorption spectra has already been documented and correlated to the dispersibility and purity of SWNTs.[31] Therefore, we think that purer and better-dispersed full-length SWNTs are obtained by the present procedure.

Very recently, Haddon et al. proposed a spectroscopic approach to quantitatively evaluate the purity of SWNTs.[36−38] We attempt to apply this method to estimate the purity of our full-length SWNTs. Figure 9 shows the solution-phase NIR absorption spectra of samples RM, NT, and NP in the range of 850−1290 nm, corresponding to the second optical absorption bands originating from semiconducting SWNTs (S_{22}). Purity calculations reveal that the relative purities of samples NT and

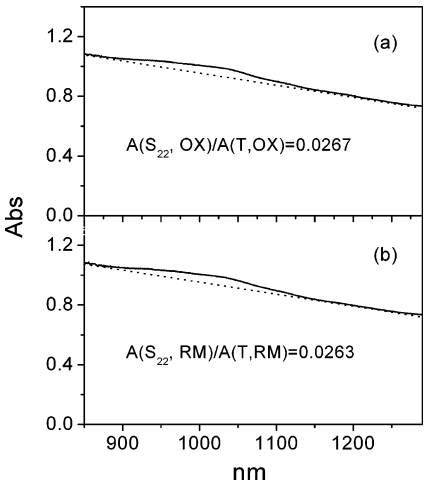

Figure 10. Absorption spectra of (a) OX dispersed in DMF and (b) RM in THF in the range of the S_{22} interband transition. *A*(T, X) and *A*(S_{22}, X) stand for the total aerial absorption and the aerial absorption of the curve X before and after baseline (dotted lines) subtraction, respectively. To account for the difference in tube concentration, the plots were normalized at 1010 nm.

NP with respect to RM are 5.1 and 1.1, respectively. This means that a 5-fold improvement in the purity of functionalized SWNTs is obtained with the dispersion−centrifugation recycles.

To estimate the real purity of our purified sample, a reference is necessary. Though a 100% pure SWNT sample is unavailable, we could estimate the purity of our functionalized full-length SWNTs with respect to the reference sample R2 in ref 36, which is an "impurity-free" fragment of soot directly from the arc chamber. The solution-phase optical absorption datum of reference sample R2 is available, which is obtained in DMF solution.[36] Our functionalized SWNTs can easily be dissolved in THF, but could not be dispersed in DMF. Thus, the solvent effect toward the absorptions has to be considered. Figure 10 shows the absorption spectra of the $K_2S_2O_8$-treated SWNT sample (OX) dispersed in DMF and the reaction mixture in THF prior to dispersion−centrifugation cycles in the range of the S_{22} interband transition. Fortunately, the absorption data of the two samples agree very well. This finding is consistent with the previous report that the S_{22} transition is much less affected by chemical processing.[36] By referencing to the documented datum *A*(S_{22}, R2)/*A*(T, R2) = 0.141, we could conclude that the relative purity of our functionalized full-length SWNTs is 96% (0.135/0.141). This means that the present procedure generates SWNTs with purity in the same level as that of the reference sample R2.

TGA was used to determine the functionalization degree and the total amount of residual metals in the samples. Figure 11 shows the TGA-DTG curves of samples AC, NT, and NP measured in argon atmosphere. It is obvious that the TG and DTG curves of the three samples show similar shapes in the same weight-loss temperature range, implying that the same component was lost during the heating process. We ascribe the weight loss to the destruction of functionalities attached on SWNTs. When heated to 500 °C, samples AC, NT, and NP undergo weight losses of 42%, 32%, and 26%, respectively, which offers a direct evidence for the different functionalization degree of the varying carbons presented in the starting material.

To estimate the amount of residual metals and the efficiency of the present purification, the samples that survived from heating in argon were successively subjected to thermogravimetric analysis in air atmosphere. As shown in Figure 12, the weight starts reducing near 350 °C and only one stepwise

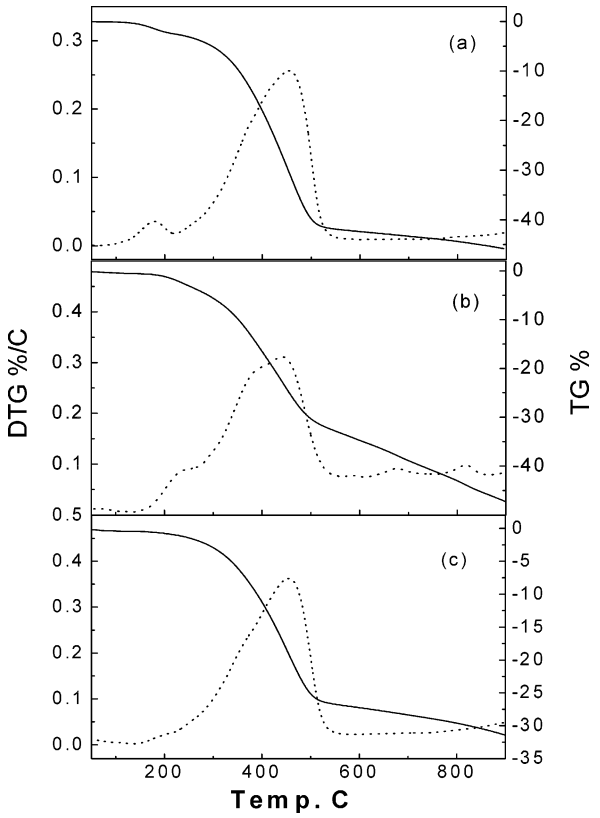

Figure 11. TGA-DTG curves of samples (a) AC, (b) NT, and (c) NP heated in argon atmosphere (ramp rate: 10 °C; Ar flow rate: 300 cm^3/min). The dotted lines represent DTG curves.

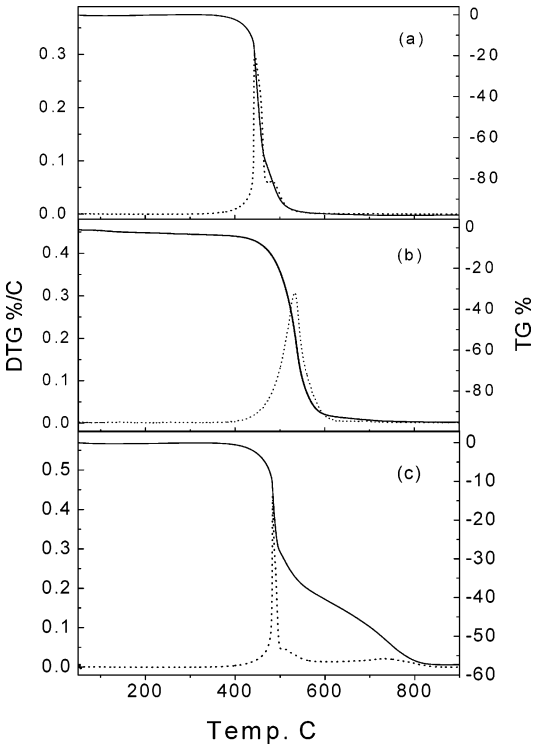

Figure 12. TGA-DTG curves of samples (a) AC, (b) NT, and (c) NP heated in air atmosphere (ramp rate: 5 °C; air flow rate: 100 cm^3/min). The dotted lines represent DTG curves.

weight-loss was observed for samples AC and NT, corresponding to the burning of amorphous carbon and SWNTs, respectively. From the DTG curve of sample NP, at least three peaks are observed. The narrow peak at 490 °C is assumed to be due

to SWNTs. The broad peak around 730 °C and the small peak near 520 °C might be because of varying crystalline graphite materials such as TSG, PCNs, etc. The burning temperature of the SWNTs in sample NP is lower than that in sample NT. This is a result of the presumably metal-catalyzed oxidation process.[11] Almost all carbon materials in these samples are burned near 900 °C, and the remaining residues are the oxidized transition metals, which are 3, 6, and 42 wt % for samples AC, NT, and NP, respectively. The much lower content of metal residue in sample NT than that in sample NP suggests an effective removal of metal catalysts from SWNTs

With the optical absorption spectroscopic and thermogravimetric data outlined above, we can estimate the SWNTs purity in samples NT (P_{NT}) and NP (P_{NP}), and then the purification efficiency factor (F_{PE}) of the present procedure.

$$P_{NT} = 96\% \times (1 - 0.785 \times 6\,\%) = 91.5\%$$

$$P_{NP} = 96\% \times 1.1/5.1 \times (1 - 0.785 \times 42\%) = 13.9\%$$

$$F_{PE} = P_{NT}W_{NT}/(P_{NT}W_{NT} + P_{NP}W_{NP}) = P_{NT}/(P_{NT} + P_{NP}W_{NP}/W_{NT}) = 91.5\%/(91.5\% + 13.9\% \times 4.3) = 60\%$$

Here W_{NT} and W_{NP} represent the sample weight of NT and NP, respectively. An average value of $W_{NP}/W_{NT} = 4.3$ was applied in calculating F_{PE}. Assuming that the TGA residue is composed of Y_2O_3 and NiO with a molar ratio of 1:4, a factor of 0.785 is introduced to calibrate the oxygen content.

4. Conclusions

In summary, we developed a procedure for nondestructive and high-yield purification of raw SWNTs, which takes advantage of chemical functionalization and supercentrifugation. From the results of SEM, Raman spectra, AFM, TEM, optical absorption, and TGA analyses, about 60% of the nanotubes in the starting material is recovered and the purity of final product is quantitatively estimated to be larger than 90 wt %. It is anticipated that both the sample purity and the recovery yield could be further improved by repeating the present purification procedure.

Acknowledgment. We thank technical assistant Makoto Fuse (National Institute of Advanced Industrial Science and Technology) for STEM measurements. This study was partly supported by Industrial Technology Research Grant Program '02 from New Energy and Industrial Technology Development Organization (NEDO) of Japan, and a Grant-in-Aid and the 21st Century COE Program from the Ministry of Education, Culture, Sports, Science and Technology.

References and Notes

(1) *Carbon nanotubes: Synthesis, Properties and Application*; Dresselhaus, M., Dresselhaus, G., Avouris, Ph., Eds.; Springer-Verlag: Berlin, 2001.
(2) Baughman, R. H.; Zakhidov, A. A.; de Heer, W. A. *Science* **2002**, *297*, 787.
(3) Shi, Z. J.; Lian, Y. F.; Zhou, X. H.; Gu, Z. N.; Zhang, Y. G.; Iijima, S.; Li, H. D.; Yue, K. T.; Zhang, S. L. *J. Phys. Chem. B* **1999**, *103*, 8698.
(4) Thess, A.; Lee, R.; Nikolaev, P.; Dai, H.; Petit, P.; Robert, J.; Xu, C.; Lee, Y. H.; Kim, S. G.; Rinzler, A. G.; Colbert, D. T.; Scuscria, G. E.; Tománek, D.; Fischer, J. E.; Smally, R. E. *Science* **1996**, *273*, 483.
(5) Bronikowski, M. J.; Willis, P. A.; Colbert, D. T.; Smith, K. A.; Smalley, R. E. *J. Vac. Sci. Technol. A* **2001**, *19*, 1800.
(6) Moon, J. M.; An, K. H.; Lee, Y. H.; Park, Y. S.; Bae, D. J.; Park, G. S. *J. Phys. Chem. B* **2001**, *105*, 5677.
(7) Dillon, A. C.; Gennett, T.; Jones, K. M.; Alleman, J. L.; Parilla, P. A.; Heben, M. J. *Adv. Mater.* **1999**, *11*, 1354.
(8) Shi, Z. J.; Lian, Y. F.; Liao, F. H.; Zhou, X. H.; Gu, Z. N.; Zhang, Y.; Iijima, S. *Solid State Commun.* **1999**, *112*, 35.
(9) Martinez, M. T.; Callejas, M. A.; Benito, A. M.; Cochet, M.; Seeger, T.; Anson, A.; Schreiber, J.; Gordon, C.; Marhic, C.; Chauvet, O.; Maser, W. K. *Nanotechnology* **2003**, *14*, 691.
(10) Tohji, K.; Takahashi, H.; Shinoda, Y.; Shimizu, N.; Jeyadevan, B.; Matsuoka, I.; Saito, Y.; Kasuya, A.; Ito, S.; Nishina, Y. *J. Phys. Chem. B* **1997**, *101*, 1974.
(11) Chiang, I. W.; Brinson, B. E.; Smalley, R. E.; Margrave, J. L.; Hauge, R. H. *J. Phys. Chem. B* **2001**, *105*, 1157.
(12) Thien-Nga, L.; Hernadi, K.; Ljubovic, E.; Garaj, S.; Forro, L. *Nano Lett.* **2002**, *2*, 1349.
(13) Banerjee, S.; Wong, S. S. *J. Phys. Chem. B* **2002**, *106*, 12144.
(14) Harutyunyan, A. R.; Pradhan, B. K.; Chang, J. P.; Chen, G. G.; Eklund, P. C. *J. Phys. Chem. B* **2002**, *106*, 8671.
(15) Vazquez, E.; Georgakilas, V.; Prato, M. *Chem. Commun.* **2002**, 2308.
(16) Bandow, S.; Rao, A. W.; Williams, K. A.; Thess, A.; Smalley, R. E.; Eklund, P. C. *J. Phys. Chem. B* **1997**, *101*, 8839.
(17) Doorn, S. K.; Strano, M. S.; O'Connell, M. J.; Haroz, E. H.; Rialon, K. L.; Hauge, R. H.; Smalley, R. E. *J. Phys. Chem. B* **2003**, *107*, 6063.
(18) Zhao, B.; Hu, H.; Niyogi, S.; Itkis, M. E.; Hamon, M. A.; Bhowmik, P.; Meier, M. S.; Haddon, R. C. *J. Am. Chem. Soc.* **2001**, *123*, 11673.
(19) Georgakilas, V.; Voulgaris, D.; Vazquez, E.; Prato, M.; Guldi, D. M.; Kukovecz, A.; Kuzmany, H. *J. Am. Chem. Soc.* **2002**, *124*, 14318.
(20) Chen, R. J.; Zhang, Y.; Wang, D.; Dai, H. *J. Am. Chem. Soc.* **2001**, *123*, 3838.
(21) Banerjee, S.; Wong, S. S. *J. Am. Chem. Soc.* **2002**, *124*, 8940.
(22) Bahr, J. L.; Tour, J. M. *J. Mater. Chem.* **2002**, *12*, 1952.
(23) Tasis, D.; Tagmatarchis, N.; Georgakilas, V.; Prato, M. *Chem. Eur. J.* **2003**, *9*, 4001.
(24) Rao, A. M.; Richter, E.; Bandow, S.; Chase, B.; Eklund, P. C.; Williams, K. A.; Fang, S.; Subbaswamy, K. R.; Menon, M.; Thess, A.; Smalley, R. E.; Dresselhaus, G.; Dresselhaus, M. S. *Science* **1997**, *275*, 187.
(25) Saito, R.; Takeya, T.; Kimura, T.; Dresselhaus, G.; Dresselhaus, M. S. *Phys. Rev. B* **1998**, *57*, 4145.
(26) Tuinstra, P.; Koenig, J. L. *J. Chem. Phys.* **1970**, *53*, 1126.
(27) Elkund, P. C.; Holden, J. M.; Jishi, R. A. *Carbon* 1**995**, *33*, 959.
(28) Laspade, P.; Marchand, A.; Couzi, M.; Cruege, F. *Carbon* **1984**, *22*, 375.
(29) Brown, S. D. M.; Corio, P.; Marucci, A.; Pimenta, M. A.; Dresselhaus, M. S.; Dresselhaus, G. *Phys. Rev. B* **2000**, *61*, 7734.
(30) Liu, J.; Rinzler, A. G.; Dai, H. J.; Hafner, J. H.; Bradley, R. K.; Boul, P. J.; Lu, A.; Iverson, T.; Shelimov, K.; Huffman, C. B.; Rodriguez-Macias, F.; Shon, Y. S.; Lee, T. R.; Colbert, D. T.; Smalley, R. E. *Science* **1998**, *280*, 1253.
(31) Lian, Y. F.; Maeda, Y.; Wakahara, T.; Akasaka, T.; Kazaoui, S.; Minami, N.; Choi, N.; Tokumoto, H. *J. Phys. Chem. B* **2003**, *107*, 12082.
(32) Dyke, C. A.; Tour, J. M. *Nano Lett.* **2003**, *3*, 1215.
(33) Kataura, H.; Kumazawa, Y.; Maniwa, Y.; Umezu, I.; Suzuki, S.; Ohtsuka, Y.; Achiba, Y. *Synth. Met.* **1999**, *103*, 2555.
(34) Chen, J.; Rao, A. M.; Lyuksyutov, S.; Itkis, M. E.; Hamon, M. A.; Hu, H.; Cohn, R. W.; Eklund, P. C.; Colbert, D. T.; Smalley, R. E.; Haddon, R. C. *J. Phys. Chem. B* **2001**, *105*, 2525.
(35) Reich, S.; Thomsen, C.; Ordejón, P. *Phys. Rev. B* **2002**, *65*, 155411.
(36) Itkis, M. E.; Perea, D. E.; Niyogi, S.; Rickard, S. M.; Hamon, M. A.; Hu, H.; Zhao, B.; Haddon, R. C. *Nano Lett.* **2003**, *3*, 309.
(37) Sen, R.; Rickard, S. M.; Itkis, M. E.; Haddon, R. C. *J. Phys. Chem. B* **2003**, *107*, 13838.
(38) Sen, R.; Rickard, S. M.; Itkis, M. E.; Haddon, R. C. *Chem. Mater.* **2003**, *15*, 4273.